P H Y S I C A L   R E V I E W   L E T T E R S

Deformation of a Trapped Fermi Gas with Unequal Spin Populations

G. B. Partridge, Wenhui Li, Y. A. Liao, and R. G. Hulet

Department of Physics and Astronomy and Rice Quantum Institute, Rice University, Houston, Texas 77251, USA

M. Haque and H. T. C. Stoof

Institute for Theoretical Physics, Utrecht University, Leuvenlaan 4, 3584 CE Utrecht, The Netherlands
(Received 29 August 2006; published 10 November 2006)

The real-space densities of a polarized strongly interacting two-component Fermi gas of ^{6}Li atoms reveal two low-temperature regimes, both with a fully paired core. At the lowest temperatures, the unpolarized core deforms with increasing polarization. Sharp boundaries between the core and the excess unpaired atoms are consistent with a phase separation driven by a first-order phase transition. In contrast, at higher temperatures the core does not deform but remains unpolarized up to a critical polarization. The boundaries are not sharp in this case, indicating a partially polarized shell between the core and the unpaired atoms. The temperature dependence is consistent with a tricritical point in the phase diagram.

The formation of pairs consisting of one spin-up and one spin-down electron underlies the phenomenon of superconductivity. While the populations of the two spin components are generally equal in superconductors, an imbalance is readily produced in experiments with gases of trapped, ultracold fermionic atoms, as was recently demonstrated [1,2]. Exotic new states of matter are predicted for the unbalanced system that, if realized, may have important implications for our understanding of nuclei, compact stars, and quantum chromodynamics. Calculations show that phase separation between pairs and the excess unpaired atoms is one possible outcome for a strongly interacting two-component gas [3–7]. We previously reported evidence for a phase separation in a trapped atomic Fermi gas to a state containing a paired central core, with the excess unpaired atoms residing outside this core [2]. Such a phase separation can be detected in the real-space distributions using *in situ* imaging, where a uniformly paired region produces a minimum in the difference distribution obtained by subtracting the majority and minority spin densities [2].

In our previous work, we noted that the excess unpaired atoms reside primarily at the axial poles of the highly elongated trap, while relatively few occupy the equatorial shell. As a result, the central minimum in the difference images was accompanied by a corresponding central dip in the axial density profile obtained by integrating the two-dimensional column density along the radial coordinate [2]. Several authors have calculated spatial distributions for phase separation, assuming both a harmonic trapping potential and the local density approximation (LDA) [8–12]. It was pointed out that, under these assumptions, a uniformly paired core would produce a constant axial density difference, rather than a central dip [13,14]. Shin *et al.* have recently adopted *in situ* imaging, and present their resulting images as evidence for phase separation, though in their experiment, no such deformation is observed [15].

In this Letter, we characterize the properties of the phase-separated state using detailed quantitative measurements of the deformation and reconstructions of the three-dimensional (3D) density distributions. Furthermore, we explore the role that finite temperature plays in determining the overall behavior of this system and identify two distinct low-temperature regimes.

Our methods for producing a strongly interacting, two-component Fermi gas of ^{6}Li atoms have been described previously [2,16]. The relative population of two hyperfine states, designated as $|1\rangle$ and $|2\rangle$, is controlled by driving radio-frequency transitions between them. Spin relaxation is negligible over the duration of the experiment. A nearly uniform magnetic field is tuned to the location of a broad Feshbach resonance at 834 G [17,18], where the two-body scattering length diverges ($\pm\infty$) producing unitarity-limited strong interactions. The combined optical and magnetic trapping potential is given by $U(r,z) = \frac{1}{2}m\omega_B^2 z^2 + U_o[1 - (\frac{w_o^2}{w^2(z)})e^{-2r^2/w^2(z)}]$, where $\omega_B = (2\pi)$ 6.5 Hz, $w_o = 26$ μm, $w(z) = w_o[1 - (z/z_o)^2]$, and $z_o = 1.7$ mm. Both radial and axial potentials are approximately harmonic for sufficiently small r and z. The atoms are evaporatively cooled by reducing the trap laser intensity until U_o achieves its final value of 540 nK. At this trap depth, the radial and axial trap frequencies are $\omega_r = (2\pi)$ 325 Hz and $\omega_z = (2\pi)$ 7.2 Hz, respectively. The two states, $|1\rangle$ and $|2\rangle$, are sequentially imaged in the trap by absorption. The first optical probe pulse breaks pairs, causing a small heating that radially broadens the second image. We have reduced the delay between probe pulses to 27 μs, significantly reducing the probe-induced broadening previously observed for delays of 215 μs [2]. Analysis of the images provides measurement of the number of atoms in each state, N_1 and N_2, from which the polarization $P = (N_1 - N_2)/(N_1 + N_2)$ is determined. Fitting the profiles of gases deliberately prepared as $P = 0$ to fermionic nonzero-temperature Thomas-Fermi distributions, gives fitted tem-

peratures of $\tilde{T} \lesssim 0.05 T_F$, where T_F is the Fermi tempera-
ture. The actual temperatures are expected to be closely
related to $\tilde{T}$ [19].

Figure 1 shows a series of images corresponding to a
range of P from 0 to 0.95. The minority spin ($|2\rangle$) distri-
bution becomes markedly less elongated with increasing P,
while its radial size remains approximately the same as that
for the majority spin ($|1\rangle$). This deformation causes the
bunching of unpaired atoms at the axial poles, and a lack of
them in the equatorial shell. Remarkably, the deformation
grows continuously with P. The central holes in the dif-
ference distributions, which are approximately equal to the
background level for all but the highest values of P,
indicate that the central core is nearly uniformly paired.
Figure 2 shows the aspect ratio for both states. While the
majority state aspect ratio changes little, that of the minor-
ity (representing the core) decreases by a factor of 10 when
going from completely unpolarized ($P = 0$) to completely
polarized ($P = 1$).

(a)   **(d)**

(b)   **(e)**

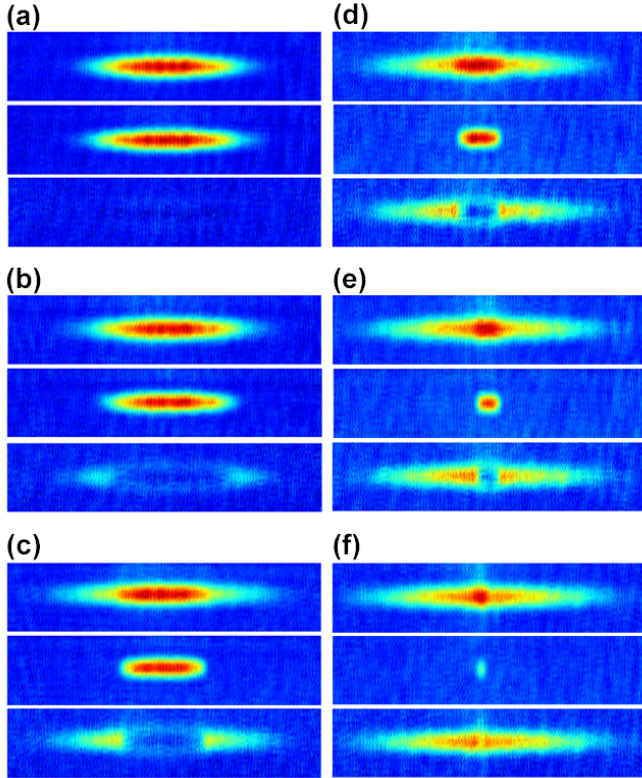**(c)**   **(f)**

FIG. 1 (color). *In situ* absorption images of a polarized Fermi
gas. The top figure of each sequence corresponds to the column
density of state $|1\rangle$, the middle to state $|2\rangle$, and the third to the
difference of the two. The polarizations are (a) $P = 0$, (b) $P =
0.18$, (c) $P = 0.37$, (d) $P = 0.60$, (e) $P = 0.79$, and (f) $P = 0.95$.
In each sequence, state $|2\rangle$ was imaged first, followed by state
$|1\rangle$. Slight probe-induced heating can be discerned in the images
of state $|1\rangle$, where the distribution bulges slightly in the radial
direction in the region of overlap between the two states. The
field of view for these images is 1654 μm by 81 μm. The
displayed aspect ratio was reduced by a factor of 4.4 for clarity.

Figure 3(a) presents a center-line cut of the column den-
sities of the majority and minority states, as well as their
difference, taken along the axial direction. The axial den-
sity difference profile of this data also exhibits a pro-
nounced central dip, as in Ref. [2]. A sharp phase bound-
ary between the core and excess fermions is readily appar-
ent in Fig. 3(a), indicating that a partially polarized shell, if
it exists, is extremely thin. Cylindrical symmetry of the
trap enables reconstruction of the true 3D density distribu-
tion $n(r, z)$ from the column densities by use of the inverse
Abel transform [20]. An axial cut of the reconstructed 3D
density, $n(r = 0, z)$, is shown in Fig. 3(b). The ratios of the
central densities, $n_1(0, 0)/n_2(0, 0)$, obtained from the re-
constructed 3D distributions, are plotted vs. P in Fig. 4(a).
The central core remains unpolarized until at least $P \approx
0.9$, in contradiction to the results reported in Ref. [15],
where uniform pairing was observed to break down at $P \approx
0.77$.

The observed LDA-violating deformations are surpris-
ing because the radial size of the distributions is about
10 times larger than the inverse Fermi momentum k_F, the
expected magnitude of the correlation length. Nonetheless,
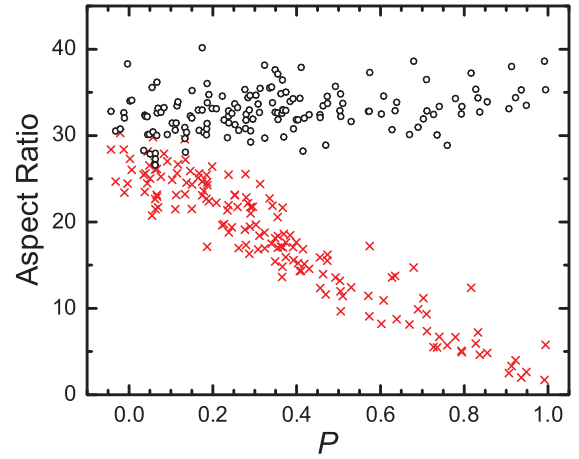several LDA-violating mechanisms, enhanced by confine-

FIG. 2 (color). Aspect ratio vs P. The ratio of the axial to the
radial dimensions, R_z/R_r, is shown for state $|1\rangle$ by the black
circles and for state $|2\rangle$ by the red crosses. The radii R_r for both
states are determined by fitting the column-density profiles to
zero-temperature, fermionic Thomas-Fermi distributions. The
axial distributions are distinctly non-Thomas-Fermi-like, so R_z
is found by a simple linear extrapolation of the column density to
zero. An aspect ratio of 36 is the expected value for a noninter-
acting gas with anharmonic corrections, in reasonable agreement
with the observations. The uncertainty in P is 0.04, which is the
standard deviation of polarization measurements deliberately
prepared as $P = 0$. There are shot-to-shot variations in N_1 and
a small systematic variation towards larger N_1 at smaller P. For
$P < 0.40$, $N_1 = (170 \pm 40) \times 10^3$, and for $P > 0.40$, $N_1 =
(135 \pm 25) \times 10^3$, where the uncertainties are the standard de-
viations of the measurements. The corresponding average Fermi
temperature is $T_F \approx 430$ nK, where we define $T_F =
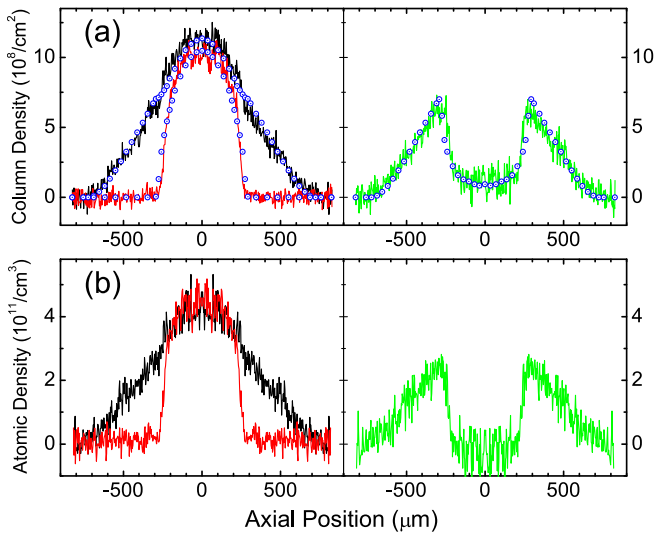\hbar(\omega_r^2 \omega_z)^{1/3}(6N_1)^{1/3}/k_B$.

FIG. 3 (color). Column-density profile and 3D density reconstruction. The black lines correspond to state $|1\rangle$, the red to state $|2\rangle$, and the green to their difference, for $P = 0.35$ and $N_1 = 175 \times 10^3$. The circles are the result of our theory (see text). (a) Center-line $(r = 0)$ axial cut of the column densities. (b) Center-line axial cut of the reconstructed 3D densities. The signal to noise of (b) was improved by reflecting and averaging the column-density images about both the $r = 0$ and the $z = 0$ planes before reconstruction. The densities in (b) are slightly diminished due to probe-induced radial broadening.

ment in a high aspect ratio trapping potential, may explain these observations. Gradient terms in the Gross-Pitaevskii equation can lead to LDA-violating deformations on the BEC side of resonance, but the magnitude of the calculated effect is much smaller than we observe at unitarity [21]. De Silva and Mueller have shown that surface tension between the normal and superfluid phases can result in deformations of the minority component that are quite similar to those observed here [22]. To quantify this, we have developed a theory for the density profiles in the gas that allows for a deformed local chemical potential that is consistent with the macroscopic deformation of the minority density profiles. The results of this calculation, the details of which will be published elsewhere, are shown in Fig. 3(a) and compare favorably with experiment. Within the limitations of our calculation, we find no evidence for a deformed Fermi surface [23] in the experimental data.

We had previously found that phase separation occurred only for $P > P_c$, where $P_c \approx 0.1$ [2]. For $P < P_c$, the observations were consistent with a non-phase-separated polarized superfluid. The present data, however, exhibit phase separation for arbitrarily small P. Since the previous work, we have improved the efficiency of the evaporation trajectory, and now obtain fitted temperatures that are about half of those previously attained. This temperature-dependent behavior is consistent with a phase boundary between a phase-separated regime and a polarized superfluid (Sarma or breached-pair phase [24–26]) at nonzero temperature. Such a phase boundary has recently been

discussed in the context of a tricritical point in the phase diagram [10,27–29]. To test this hypothesis, we deliberately produced higher temperatures by stopping the evaporation trajectory at a higher trap depth (1.2 μK), resulting in $\tilde{T} \approx 0.2T_F$. Figure 4(b) shows that the central densities in this case remain equal until a critical polarization of $P \approx 0.6$–0.7 is reached.

Figure 5 shows absorption images prepared at both the lower and higher temperatures. It is readily apparent from the images that the density distributions of the two components of the higher temperature gas show no deformations, in contrast to those of the colder case. We find that at higher temperatures, the aspect ratios of the minority and majority components remain equal and constant for all P. This lack of deformation is also evident in the axial density distributions, where in the case of the colder data, the axial difference distribution [Fig. 5(b)] shows the characteristic double-peaked structure observed previously [2], while that of the warmer cloud [Fig. 5(d)] exhibits the flat-topped distribution reported in Ref. [15] and expected for a paired core with no deformation [13,14]. The phase boundary is also much sharper for the low-temperature data. In summary, the higher temperature data support the suggestion of a temperature-dependent transition between a low-temperature phase-separated state and a higher temperature polarized superfluid [28,29].

We have reported that pairing with unequal spin populations leads to real-space deformations in a highly elon-
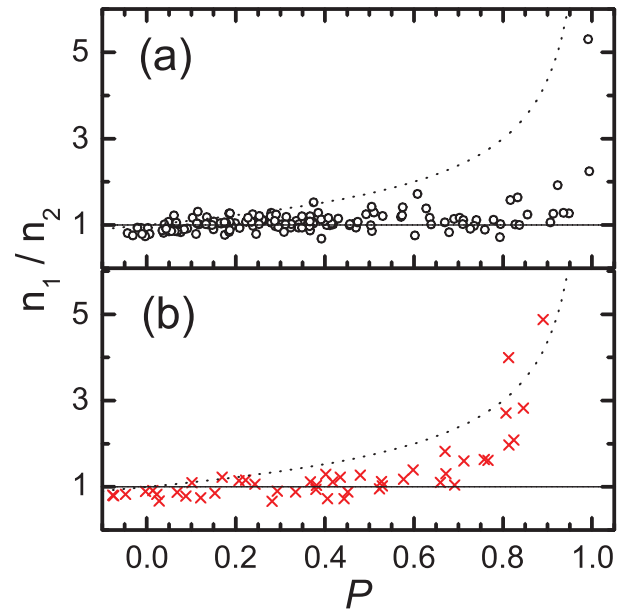

FIG. 4 (color). Ratio of the central densities vs polarization. (a) $\tilde{T} \lesssim 0.05T_F$, corresponding to the data shown in Fig. 2; (b) $\tilde{T} \approx 0.2T_F$, with average $N_1 = 500 \times 10^3$. The dotted lines correspond to $[(1 + P)/(1 - P)]^{1/2}$, the expected central density ratio for a harmonically confined, noninteracting gas at $T = 0$. The increase in $n_1(0, 0)/n_2(0, 0)$ in (a) for $P > 0.9$ may be explained by higher temperatures for these data that arise from inefficiencies in evaporative cooling at very high P.
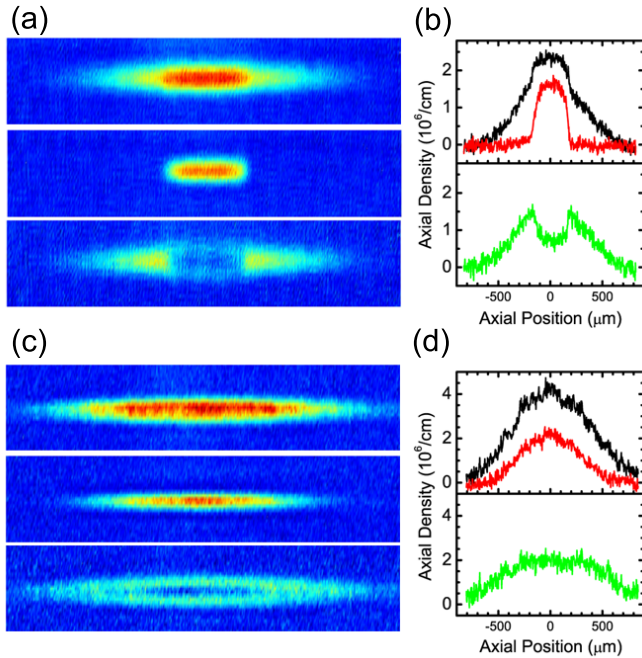
FIG. 5 (color). *In situ* absorption images and integrated profiles. To the left are absorption images, while the plots to the right are the corresponding axial density distributions. (a),(b): $P = 0.50$, $N_1 = 146 \times 10^3$, with $\tilde{T} \lesssim 0.05 T_F$; (c),(d): $P = 0.45$, $N_1 = 374 \times 10^3$, with $\tilde{T} \approx 0.2 T_F$. The central bulge evident in the state $|1\rangle$ density in (b) is indicative of strong attraction between atoms in the core region.

gated, but still three-dimensional geometry. The sharp phase boundaries between the superfluid core and the polarized normal phase are consistent with the usual convention that phase separation is associated with first-order phase transitions. At elevated temperatures, but still below the transition to the normal state, deformations are absent, and a partially polarized shell is observed between a uniformly paired core and the fully polarized outer shell. These observations support the existence of a tricritical point in the phase diagram where the superfluid-normal transition changes from second-order to first-order as the temperature is lowered.

[1] M. W. Zwierlein, A. Schirotzek, C. H. Schunck, and W. Ketterle, Science **311**, 492 (2006).
[2] G. B. Partridge, W. Li, R. I. Kamar, Y. A. Liao, and R. G. Hulet, Science **311**, 503 (2006).
[3] P. F. Bedaque, H. Caldas, and G. Rupak, Phys. Rev. Lett. **91**, 247002 (2003).
[4] J. Carlson and S. Reddy, Phys. Rev. Lett. **95**, 060401 (2005).
[5] D. E. Sheehy and L. Radzihovsky, Phys. Rev. Lett. **96**, 060401 (2006).
[6] Z.-C. Gu, G. Warner, and F. Zhou, cond-mat/0603091.
[7] H. Hu and X.-J. Liu, Phys. Rev. A **73**, 051603(R) (2006).
[8] P. Pieri and G. C. Strinati, Phys. Rev. Lett. **96**, 150404 (2006).
[9] W. Yi and L.-M. Duan, Phys. Rev. A **73**, 031604(R) (2006).
[10] F. Chevy, Phys. Rev. Lett. **96**, 130401 (2006).
[11] C.-H. Pao and S.-K. Yip, J. Phys. Condens. Matter **18**, 5567 (2006).
[12] C.-C. Chien, Q. Chen, Y. He, and K. Levin, Phys. Rev. A **74**, 021602(R) (2006).
[13] T. N. De Silva and E. J. Mueller, Phys. Rev. A **73**, 051602(R) (2006).
[14] M. Haque and H. T. C. Stoof, Phys. Rev. A **74**, 011602(R) (2006).
[15] Y. Shin, M. W. Zwierlein, C. H. Schunck, A. Schirotzek, and W. Ketterle, Phys. Rev. Lett. **97**, 030401 (2006).
[16] G. B. Partridge, K. E. Strecker, R. I. Kamar, M. W. Jack, and R. G. Hulet, Phys. Rev. Lett. **95**, 020404 (2005).
[17] M. Houbiers, H. T. C. Stoof, W. I. McAlexander, and R. G. Hulet, Phys. Rev. A **57**, R1497 (1998).
[18] M. Bartenstein *et al.*, Phys. Rev. Lett. **94**, 103201 (2005).
[19] J. Kinast, A. Turlapov, J. E. Thomas, Q. Chen, J. Stajic, and K. Levin, Science **307**, 1296 (2005).
[20] L. M. Smith, D. R. Keefer, and S. I. Sudharsanan, J. Quant. Spectrosc. Radiat. Transfer **39**, 367 (1988).
[21] A. Imambekov, C. J. Bolech, M. Lukin, and E. Demler, cond-mat/0604423.
[22] T. N. De Silva and E. J. Mueller, Phys. Rev. Lett. **97**, 070402 (2006).
[23] A. Sedrakian, J. Mur-Petit, A. Polls, and H. Müther, Phys. Rev. A **72**, 013613 (2005).
[24] G. Sarma, J. Phys. Chem. Solids **24**, 1029 (1963).
[25] M. Houbiers, R. Ferwerda, H. T. C. Stoof, W. I. McAlexander, C. A. Sackett, and R. G. Hulet, Phys. Rev. A **56**, 4864 (1997).
[26] W. V. Liu and F. Wilczek, Phys. Rev. Lett. **90**, 047002 (2003).
[27] R. Combescot and C. Mora, Europhys. Lett. **68**, 79 (2004).
[28] M. M. Parish, F. M. Marchetti, A. Lamacraft, and B. D. Simons, cond-mat/0605744.
[29] K. B. Gubbels, M. W. J. Romans, and H. T. C. Stoof, cond-mat/0606330.